Electronic Supplementary Material (ESI) for Analyst.

Supporting Information for

LA-ICP-MS and MALDI-MS image registration for correlating nanomaterial biodistributions and their biochemical effects

Laura J. Castellanos-Garcia, Kristen N. Sikora, Jeerapat Doungchawee, and Richard W. Vachet*

Department of Chemistry, University of Massachusetts Amherst

Supplemental Methods:

Chemicals and Materials. Arginine, 1-pentanthiol, and linoleic acid were purchased from Sigma-Aldrich (St. Louis, MO). Chloroauric acid for gold nanoparticle (AuNP) synthesis was bought from Strem Chemicals Inc. (Newburyport, MA). siRNA targeting TNF-α with the sequence: 5′-GUCUCAGCCUCUUCUCAUUCCUGct-3′ (sense strand) was synthesized by Sigma-Aldrich. Phosphate-buffered saline (PBS) was purchased from Fisher Scientific.

Nanoparticle and NPSC Synthesis and Characterization. The arginine-functionalized AuNPs (Arg-AuNPs) that comprise the nanoparticle-stabilized capsules, and the NPSCs themselves were synthesized as previously described.[1] In brief, 1-pentanethiol protected AuNPs (Au-C5) with ~2 nm core diameters were synthesized using the Brust-Schiffrin two-phase synthesis.[2] Arginine-functionalized thiol ligands were synthesized using the method in a previous report.[3] The arginine-functionalized thiol ligands were then attached to the AuNP core by the Murray place-exchange method.[4] To form the NPSCs, 1 μL of linoleic acid was combined with 1 μM Arg-AuNPs in PBS. Emulsions were formed by using an amalgamator at 5000 rpm for 100 s. 10 μL of the emulsion was combined with a mixture of 2.5 μM Arg-AuNPs and 1 μM siRNA (90 μL in 5 mM phosphate buffer). The mixture was incubated for 10 min at room temperature.

Characterization of the NPSCs and Arg-AuNPs followed procedures that have been previously reported.[5,6] Dynamic light scattering (DLS) measurements were performed using a Malvern Zetasizer, and the results are summarized in Table S1. Transmission electron microscopy and other data for these materials can be found elsewhere,[5] as the exact same materials that were used in that study were used in the current study.

Table S1. Physical characteristics of anti-TNF-α NPSCs and Arg-AuNPs measured by dynamic light scattering (DLS).

Particle Type	Hydrodynamic Diameter (nm)	Polydispersity Index	Zeta Potential (mV)
Arg-AuNPs	11 ± 1	0.26 ± 0.01	+15.1 ± 0.2
Anti-TNF-α NPSCs	179 ± 3	0.24 ± 0.01	-3.3 ± 0.1

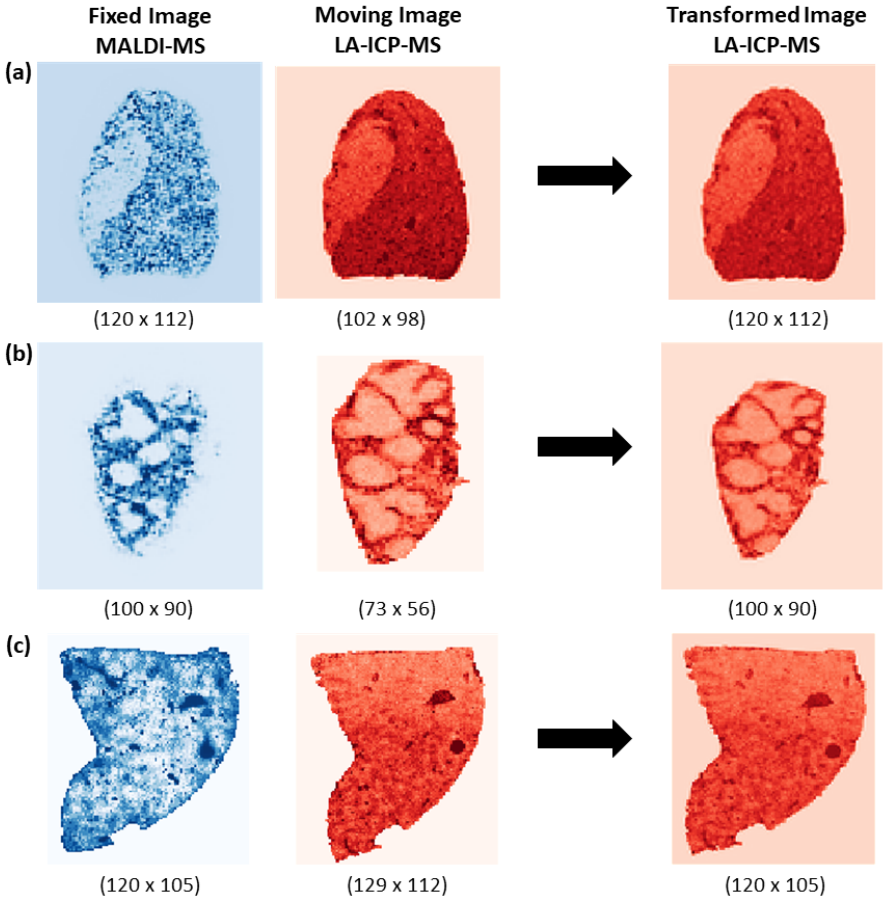

Figure S1. Fixed, moving, and transformed images for (a) mouse liver sections analyzed by MALDI-MS, with matrix deposition via the ImagePrep matrix sprayer, and LA-ICP-MS, (b) mouse spleen sections analyzed by MALDI-MS, with matrix deposition via the ImagePrep matrix sprayer, and LA-ICP-MS, and (c) mouse liver sections analyzed by MALDI-MS, with matrix deposition via sublimation, and LA-ICP-MS. The numbers at the bottom of image represent the pixel dimensions of the given image. The pixel dimensions of the moving image are transformed into the same coordinate system as the fixed image.

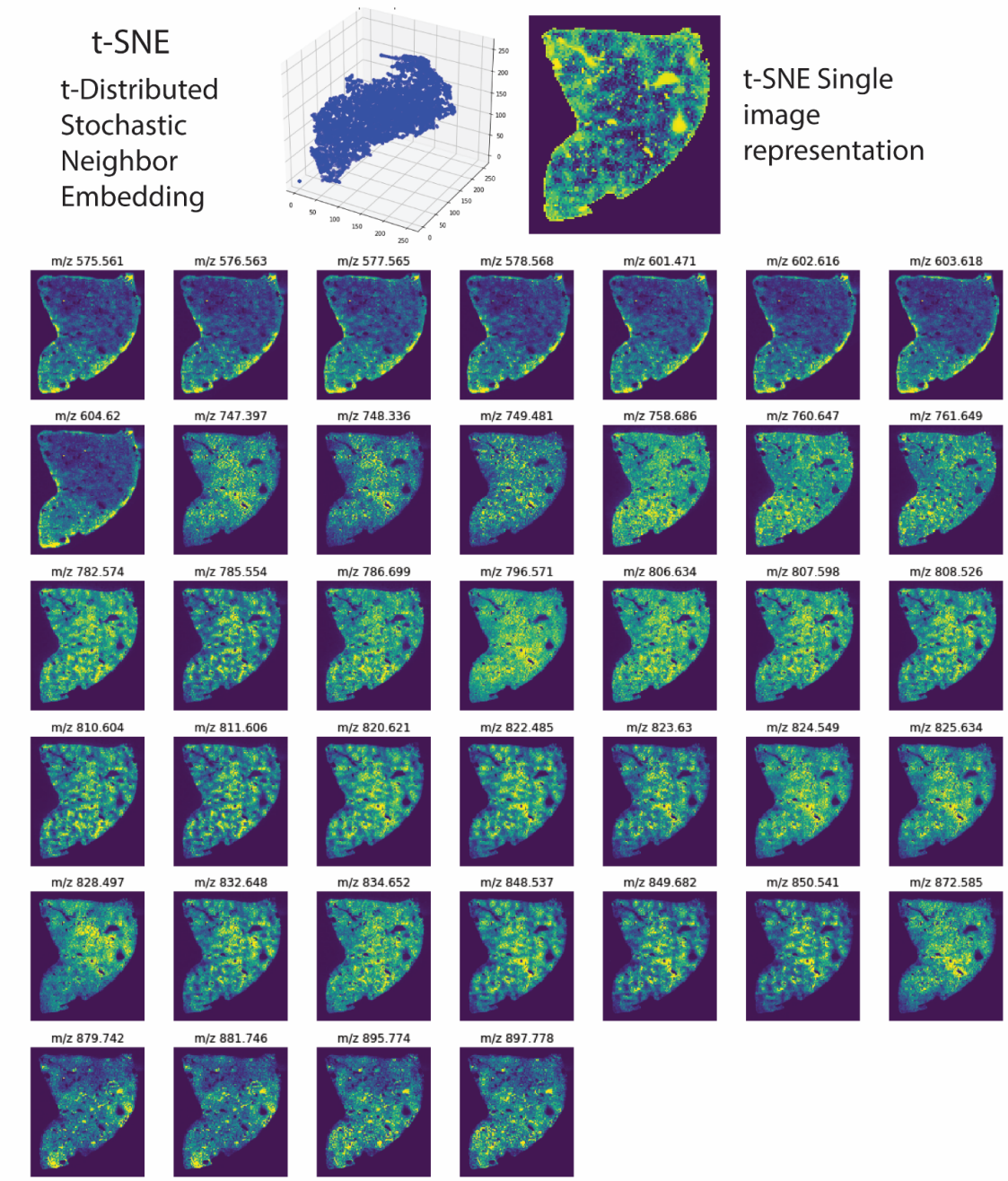

Figure S2. MALDI-MS images from a mouse liver tissue section, showing different lipid ion images that were used as input to reduce the dimensionally of the MALDI-MS dataset by t-distributed stochastic neighbor embedding (t-SNE).

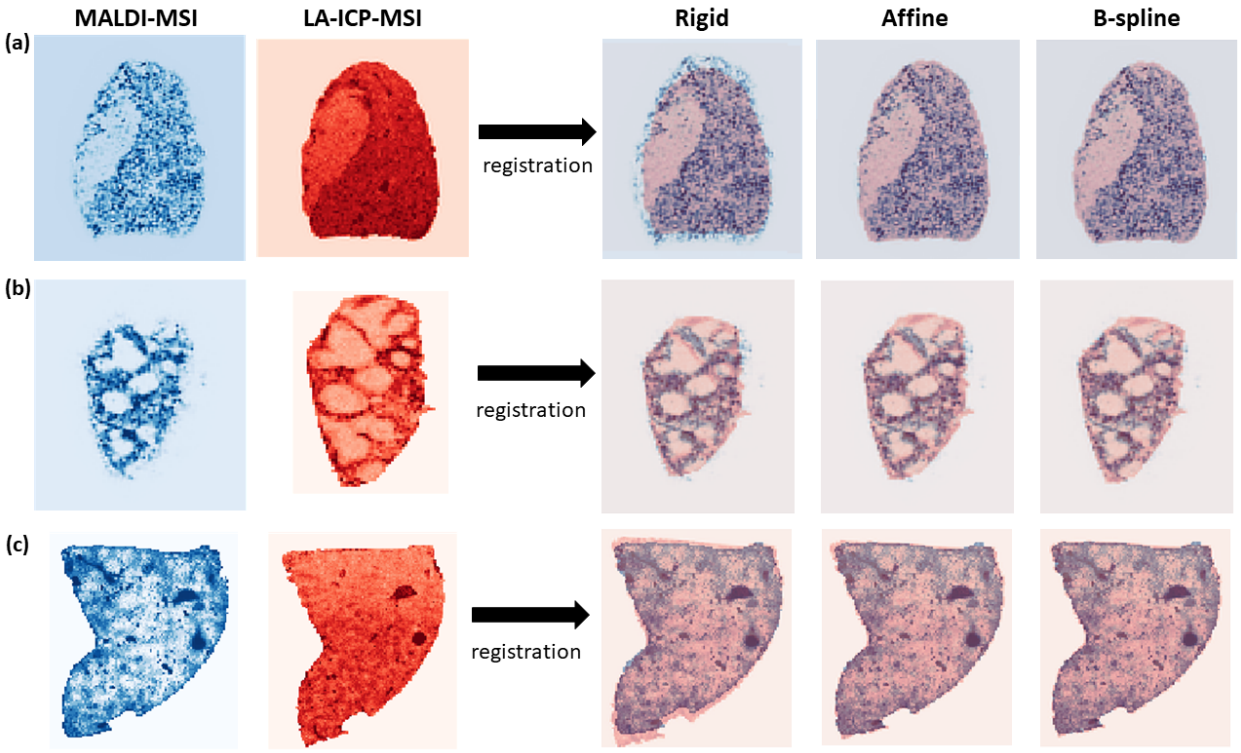

Figure S3. Examples of rigid, affine, and B-spline transformation parameters for registering MALDI-MS and LA-ICP-MS images of liver (a and c) and spleen tissues from mice. Rigid transformations involve translating or rotating images for better overlap. Affine transformations add scaling and skewing factors for images that are different sizes. B-spline uses non-linear transformation that compensate for localized distortions.

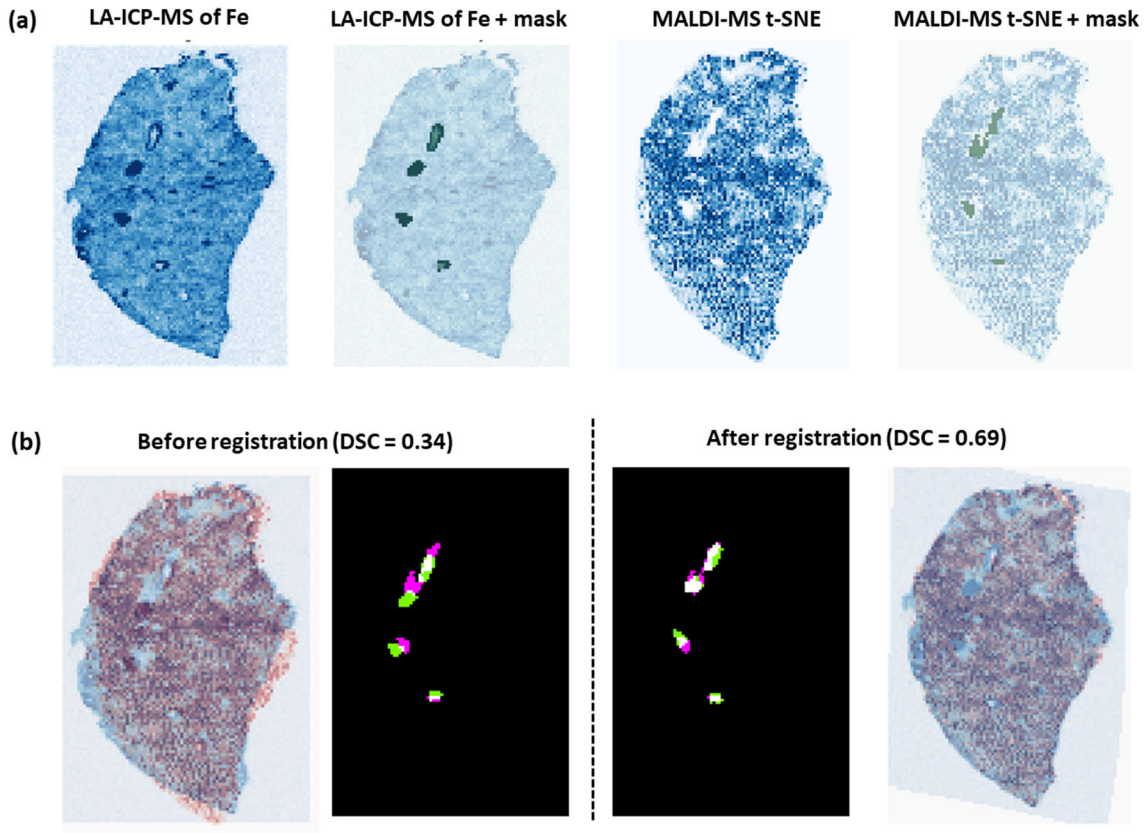

Figure S4. Registration validation using DSC calculations for non-adjacent mouse liver tissue sections. (a) LA-ICP-MS and MALDI-MS images and masks before registration. (b) Overlay of vein masks and DSC values, before and after registration. Green = LA only pixels, Magenta = MALDI only pixels, White = Overlay pixels. Segmentation of the veins was performed manually using the Fe image in LA-ICP-MS and the t-SNE image in MALDI-MS to generate computational masks for each of the two images.

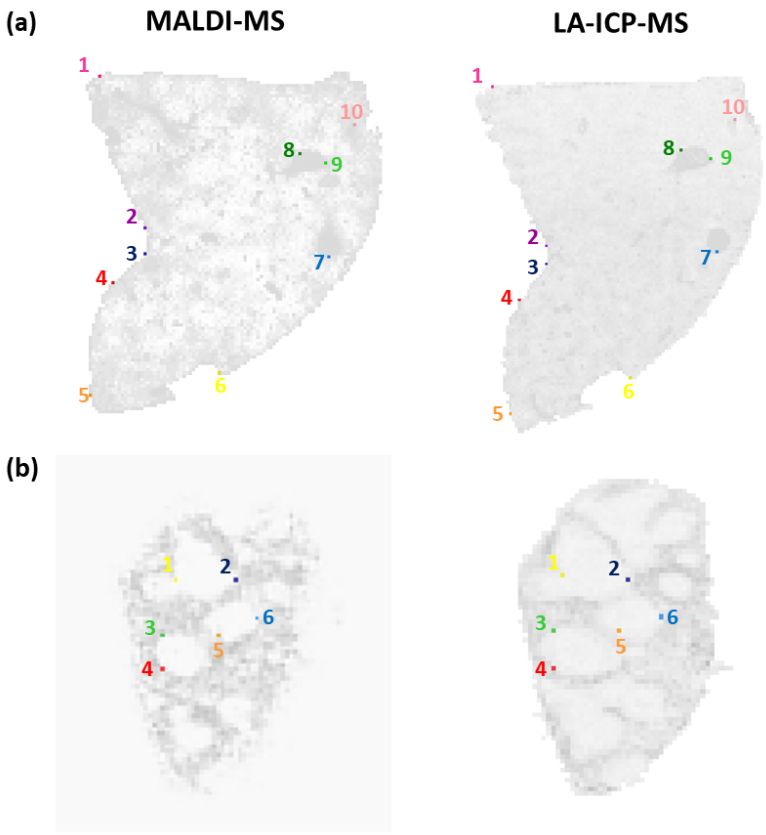

Figure S5. Landmark validation of LA-ICP-MS and MALDI-MS registration using selected pixels corresponding to morphologically distinct sites in (a) liver and (b) spleen tissues in mice. The numbers indicate the pixels that were chosen as landmarks in both imaging modalities. In the landmark validation process, the images are overlaid, and the Euclidean distance between corresponding points is measured to determine the registration accuracy.

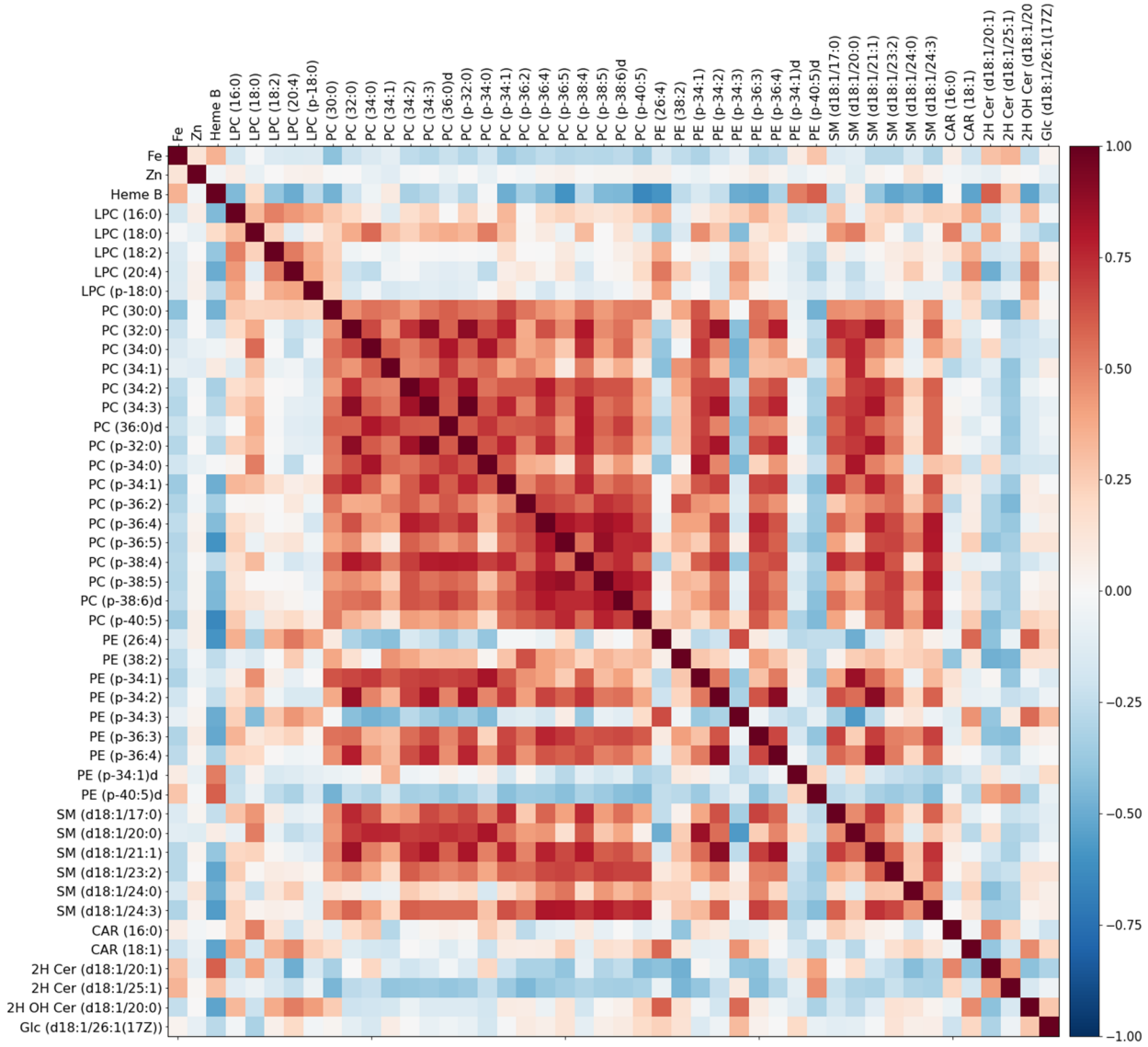

Figure S6. Correlation map plot for a spleen control mouse, showing correlations among the LA-ICP-MSI analytes (Fe, Zn), with the lipids detected by MALDI-MSI.

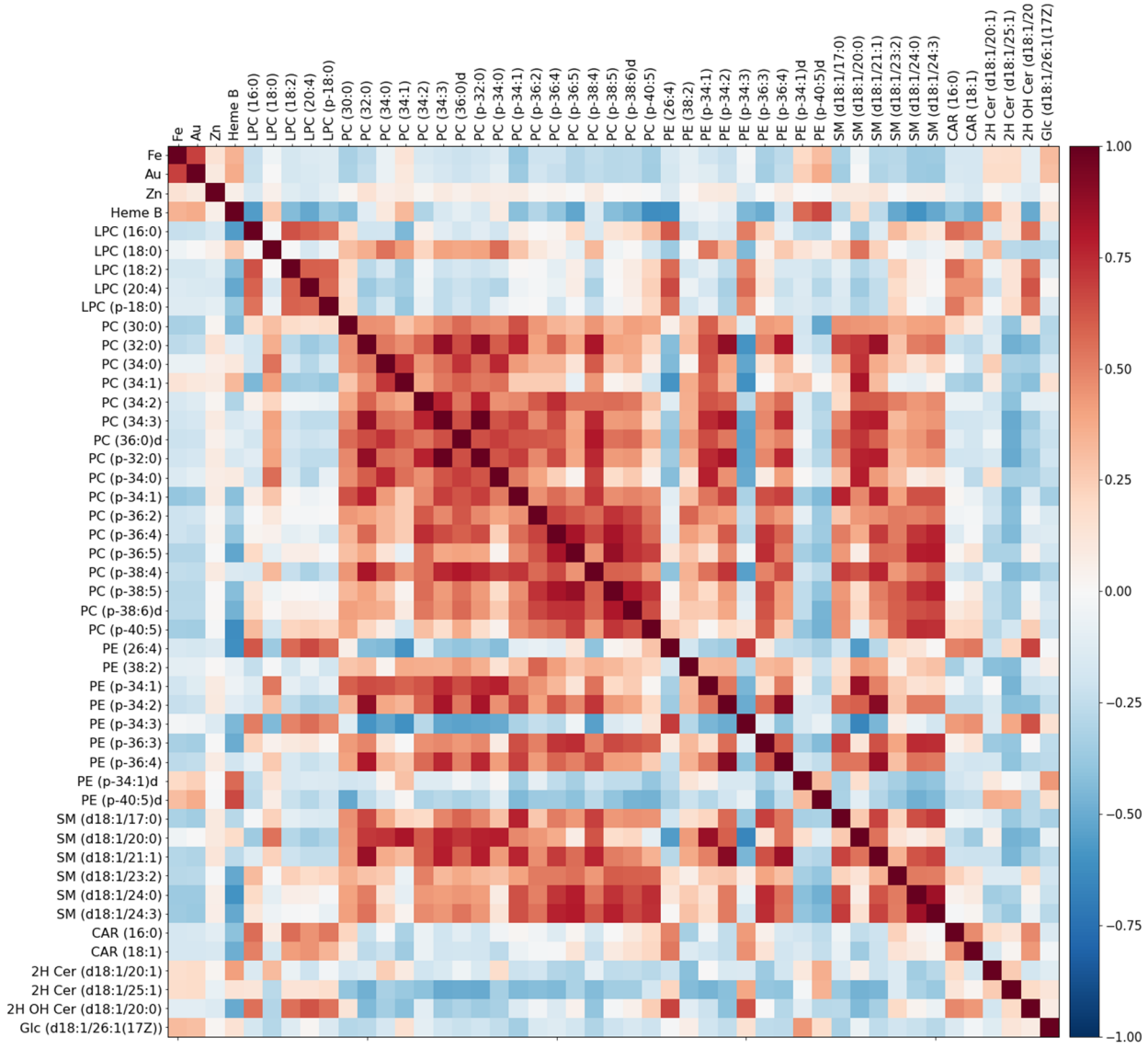

Figure S7. Correlation map plot for a spleen from a NPSC-injected mouse, showing correlations among the LA-ICP-MS analytes (Au, Fe, Zn) with the lipids detected by MALDI-MS.

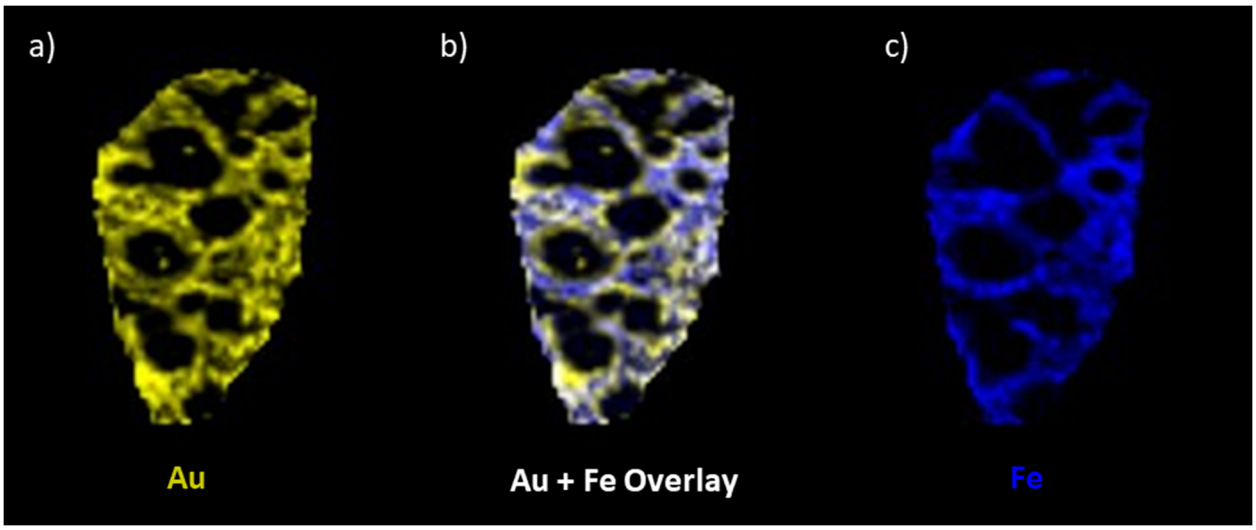

Figure S8. Overlay of Au and Fe signals from a spleen tissue from a NPSC-treated mouse (b). The Au image shows nanomaterial accumulation in the red pulp of the spleen (a), and the Fe image distinguishes the areas between red and white pulp using blood as marker of the suborgan regions (c).

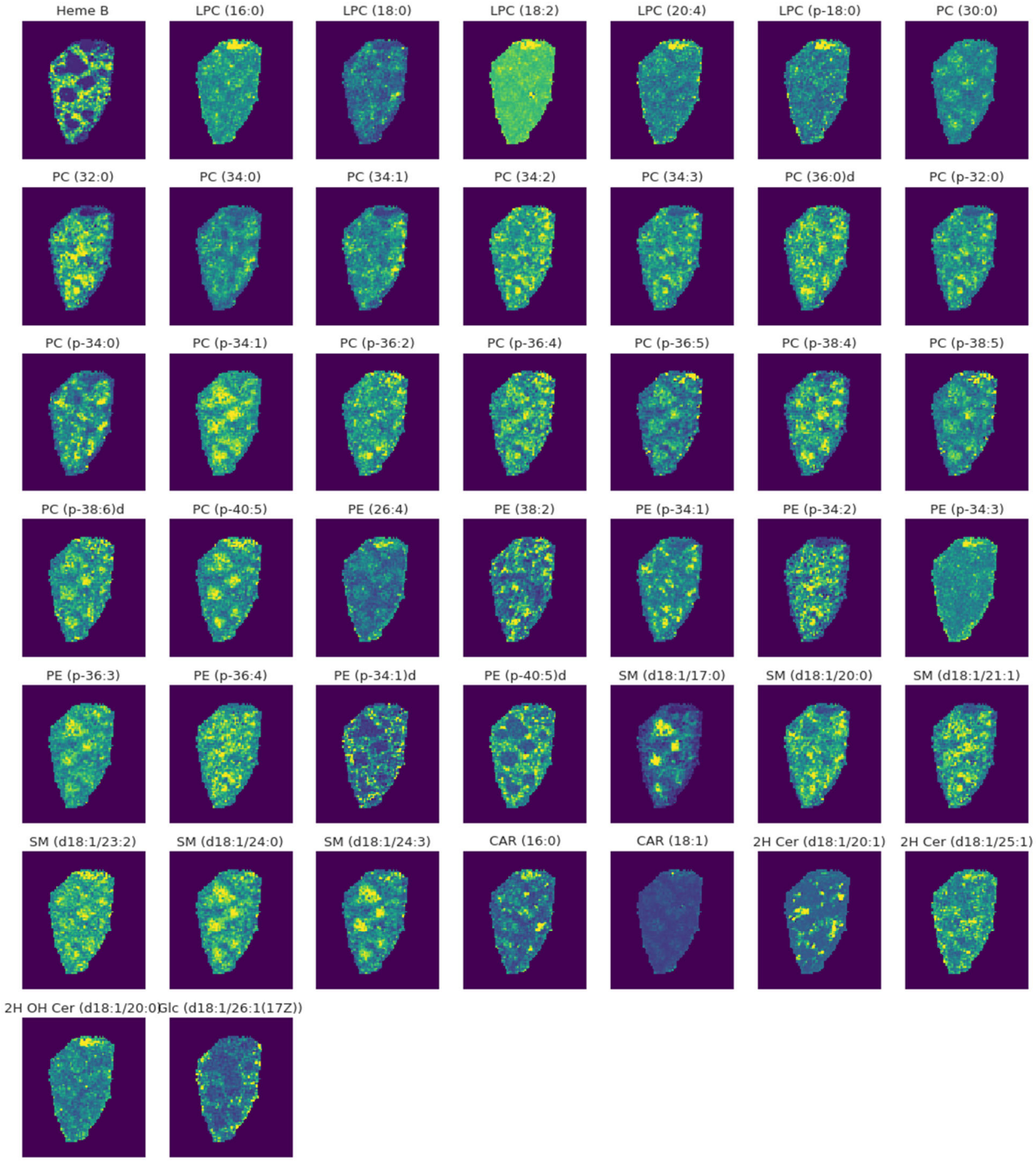

Figure S9. MALDI images of the detected lipids on spleen tissue NPSC injected.

SI References

1. Yang, X.-C.; Samanta, B.; Agasti, S. S.; Jeong, Y.; Zhu, Z.-J.; Rana, S.; Miranda, O. R.; Rotello, V. M. Drug Delivery Using Nanoparticle-Stabilized Nanocapsules. *Angew. Chemie Int. Ed.* **2011**, *50* (2), 477–481.

2. Brust, M.; Walker, M.; Bethell, D.; Schiffrin, D. J.; Whyman, R. Synthesis of Thiol-Derivatised Gold Nanoparticles in a Two-Phase Liquid–Liquid System. *J. Chem. Soc., Chem. Commun.* **1994**, No. 7, 801–802.
3. Miranda, O. R.; Chen, H.-T.; You, C.-C.; Mortenson, D. E.; Yang, X.-C.; Bunz, U. H. F.; Rotello, V. M. Enzyme-Amplified Array Sensing of Proteins in Solution and in Biofluids. *J. Am. Chem. Soc.* **2010**, *132* (14), 5285–5289.
4. Hostetler, M. J.; Templeton, A. C.; Murray, R. W. Dynamics of Place-Exchange Reactions on Monolayer-Protected Gold Cluster Molecules. *Langmuir* **1999**, *15* (11), 3782–3789.
5. Jiang, Y.; Hardie, J.; Liu, Y.; Ray, M.; Luo, X.; Das, R.; Landis, R. F.; Farkas, M. E.; Rotello, V. M.; Nanocapsule-Mediated Cytosolic SiRNA Delivery for Anti-Inflammatory Treatment. *J. Control. Release* **2018**, *283*, 235–240.
6. Hardie, J.; Jiang, Y.; Tetrault, E. R.; Ghazi, P. C.; Tonga, G. Y.; Farkas, M. E.; Rotello, V. M. Simultaneous Cytosolic Delivery of a Chemotherapeutic and siRNA Using Nanoparticle-Stabilized Nanocapsules. *Nanotechnology* **2016**, *27*, 374001.